

Ensemble-Based Graph Representation of fMRI Data for Cognitive Brain State Classification

Daniil Vlasenko, Vadim Ushakov, Alexey Zaikin, Denis Zakharov

Abstract—Understanding and classifying human cognitive brain states based on neuroimaging data remains one of the foremost and most challenging problems in neuroscience, owing to the high dimensionality and intrinsic noise of the signals. In this work, we propose an ensemble-based graph representation method of functional magnetic resonance imaging (fMRI) data for the task of binary brain-state classification. Our method builds the graph by leveraging multiple base machine-learning models: each edge weight reflects the difference in posterior probabilities between two cognitive states, yielding values in the range $[-1, 1]$ that encode confidence in a given state. We applied this approach to seven cognitive tasks from the Human Connectome Project (HCP 1200 Subject Release), including working memory, gambling, motor activity, language, social cognition, relational processing, and emotion processing. Using only the mean incident edge weights of the graphs as features, a simple logistic-regression classifier achieved average accuracies from 97.07% to 99.74%. We also compared our ensemble graphs with classical correlation-based graphs in a classification task with graph neural network (GNN). In all experiments, the highest classification accuracy was obtained with ensemble graphs. These results demonstrate that ensemble graphs convey richer topological information and enhance brain-state discrimination. Our approach preserves edge-level interpretability of the fMRI graph representation, is adaptable to multiclass and regression tasks, and can be extended to other neuroimaging modalities and pathological-state classification.

Index Terms—fMRI, functional connectivity, networks, ensemble learning, GNN, classification.

I. INTRODUCTION

One of the central objectives of modern interdisciplinary science is to study the fundamental principles underlying human brain functioning. Nowadays, the primary approach involves studying brain activity through various neuroimaging

techniques, such as electroencephalography (EEG), magnetoencephalography (MEG), and functional magnetic resonance imaging (fMRI), to identify functional brain networks responsible for specific cognitive processes. Importantly, previous work has shown that the choice of neuroimaging data representation, whether at the sensor, source, or graph level, can significantly affect the outcome of brain-state classification tasks across different modalities [2]–[4]. Understanding how different brain regions interact and coordinate their activity during various cognitive tasks, as well as the ability to accurately classify brain states, can provide significant insights into the nature of cognitive processes and aid in the development of diagnostic and therapeutic methods for neurodegenerative diseases. In this context, fMRI has become a key tool for mapping brain activity and analyzing cognitive states [5], [6].

Analysis of fMRI data is a challenging task due to its high dimensionality and dynamic nature. In recent years, increasing attention has been devoted to applying network-based methods to represent functional connectivity between different brain regions (see, e.g. [7]–[9]). These methods describe the brain activity using a functional network, where nodes represent brain regions, and edges correspond to functional connections between them. This approach enables a more comprehensive understanding of cognitive states by identifying both local and global connectivity patterns in brain activity. Moreover, using network-based methods for fMRI data analysis allows not only for the investigation of brain network characteristics but also for exploring their topology with machine learning techniques (see, e.g. [10]–[13]), which is impossible with classical statistical methods.

Currently, there are several methods for representing fMRI data in network form. The simplest and most widely used method is correlation-based graphs [10], [12], [14] that use Pearson's correlation coefficients as edge weights. In general, functional connectivity between two brain regions can be computed using any metric that may or may not be invariant to time and spatial positioning of brain regions [15]–[17].

In [18], we merely proposed the idea of using ensemble learning [19]–[21] to construct connectivity graphs for a wide range of neuroimaging data. In this paper, we build on that concept by providing the first complete, step-by-step description of the method, implementing it in practice, and empirically validating its performance for fMRI data. Thus this work represents the first fully operational and tested realization of the framework we introduced earlier. This approach is designed for binary brain state classification and offers several significant advantages. First, ensemble learning effectively

The research was supported by the Russian Science Foundation (grant number 24-68-00030) and in part through computational resources of HPC facilities at NRU HSE [1].

Daniil Vlasenko, Vadim Ushakov, Alexey Zaikin, Denis Zakharov are with Institute for Cognitive Neuroscience of University Higher School of Economics, 20 Myasnitskaya St., Moscow, 101000, Russia, (dvlasenko@hse.ru, vushakov@hse.ru, alexey.zaikin@ucl.ac.uk, dgzakharov@hse.ru).

Alexey Zaikin is with Department of Mathematics and Institute for Women's Health of University College London, London, WC1H 0AY, UK, (alexey.zaikin@ucl.ac.uk).

Corresponding author: Daniil Vlasenko (dvlasenko@hse.ru).

Preprint. This work has been submitted to the IEEE for possible publication. Copyright may be transferred without notice, after which this version may no longer be accessible.

handles noise inherent in neuroimaging data and inter-subject variability in cognitive processes. Second, preprocessing data using machine learning techniques before employing a complex classification model improves classification accuracy. Third, our method of representing fMRI data allows for the integration of multimodal data and captures valuable information provided by different connectivity metrics and regional time series characteristics. By combining the advantages of various metrics into a single graph, our method reduces memory consumption and computational time required for subsequent network analysis. We called such graphs ensemble or synolitic graphs, derived from the Greek word “synolo,” meaning ensemble [22].

To test the effectiveness of the method, we constructed ensemble graphs on fMRI data from the Human Connectome Project (HCP) 1200 Subject Release [23], [24] and performed classification of brain states using logistic regression on node features. In seven experiments on different cognitive tasks (working memory, gambling, motor task, language processing, social cognition, relational processing, and emotional processing), classification accuracy ranged from 97.07 % to 99.74 %. This indicates that even a simple model based on the features of ensemble graph nodes can reliably distinguish between the two brain states. We also compared the performance of our method in the classification task with correlation graphs using a graph neural network (GNN). Using the same GNN architecture, ensemble graphs provided an average classification accuracy ranging from 88.00 % to 99.42 %, while correlation graphs performed significantly worse: from 61.86 % to 97.94 %. In all seven tasks, ensemble graphs showed the best performance, which emphasizes the advantage of our approach of network representation of fMRI data for classification task.

II. METHODS

A. Data and Preprocessing

Data were obtained from the Human Connectome Project, specifically the HCP 1200 Subject Release [23], [24]. From this dataset, we selected 581 healthy participants, comprising 295 women and 286 men, aged 22 to 35 years. All selected participants had no anatomical abnormalities reported by HCP and had completed all fMRI experiments. The experiments were designed to activate various cortical and subcortical brain networks and included tasks focused on working memory, gambling, motor activity, language processing, social cognition, relational processing, and emotion processing [25].

fMRI data acquisition was performed using a 3T MRI scanner with the following parameters: 208 mm × 180 mm field of view, 2.0 mm isotropic voxel size, a repetition time (TR) of 0.72 seconds, an echo time (TE) of 33.1 milliseconds, and a flip angle of 52 degrees. For our analysis, we utilized data with only the right-to-left phase encoding direction to maintain consistency. Data preprocessing followed the HCP minimal preprocessing pipeline, addressing motion correction, magnetic field distortion correction, spatial normalization, and filtering of spatial and temporal noise. For more details about data acquisition and HCP minimal preprocessing pipeline see [25], [26].

We performed additional preprocessing steps, including linear trend removal and standardization (z-scoring) of voxel time series. Brain parcellation into 379 regions was achieved using the [27] multi-modal parcellation atlas. Among these regions, 180 were located in the cortex of each hemisphere, and an additional 19 were subcortical regions. After parcellation, two approaches were used to obtain representative time series for each region: (1) voxel time series within each region were averaged, and (2) principal component analysis (PCA) was applied, with the first principal component extracted as the representative time series. These two approaches resulted in two separate datasets, allowing us to evaluate our method on both averaged time series and PCA-based representations independently.

After preprocessing for each of the seven experiments, we determined two distinct brain states corresponding to different cognitive tasks (Table I). The final dataset comprised 1162 labeled samples per experiment.

TABLE I

TWO BRAIN STATES FOR EACH COGNITIVE TASK, BETWEEN WHICH CLASSIFICATION IS MADE.

	state 1	state 2
Working Memory	0-back	2-back
Gambling	win	loss
Motor Activity	left arm or leg	right arm or leg
Language Processing	story	math
Social Cognition	random movement	mental iterations
Relational Processing	relation	match
Emotion Processing	neutral	fear

B. Graph Representation of fMRI Data.

We defined a complete undirected weighted graph $g = (V, E, H, W)$, where $V = \{i | i \in 1, \dots, n\}$ represents the set of vertices, $E = \{ij | i \in V; j \in V; i \neq j\}$ represents the set of undirected edges, $H = \{h_i | i \in V\}$ denotes the vectors of values associated with vertices, and $W = \{w_{ij} | ij \in E\}$ denotes the weights of the edges. Each vertex corresponds to a brain region derived from the parcellation of fMRI data. The time series of a brain region i is denoted by x_i .

1) *Correlation Graphs*: To provide a baseline for comparison, we constructed correlation graphs. In these graphs each vertex vector of values h_i corresponds to the mean value and standard deviation of the region’s time series: $h_i = (\text{mean}(x_i), \text{std}(x_i))$. The edge weight w_{ij} is computed as the Pearson correlation coefficient between the time series of regions i and j : $w_{ij} = \rho(x_i, x_j)$. To ensure consistency, the edge weights in each graph were standardized (z-scored).

2) *Ensemble Graphs*: For ensemble graphs, the edge weight w_{ij} represents the difference in probabilities of the two brain states, given a set of functions f_1, \dots, f_k of the time series of regions i and j :

$$w_{ij} = P(2 | f_1(x_i, x_j), \dots, f_k(x_i, x_j)) - P(1 | f_1(x_i, x_j), \dots, f_k(x_i, x_j)). \quad (1)$$

In our study the chosen functions f_1, \dots, f_k included the mean values and standard deviations of the time series of

regions i and j and the Pearson correlation coefficient between their time series. Pearson correlation coefficients were standardized (z-scored) as in correlation graphs before used in (1). These metrics were selected for two main reasons. First, they are straightforward and widely used measures, making the resulting graphs easier to interpret and analyze. Second, by using the same information (mean values and correlations) as inputs for the ensemble graphs, we ensured a fair comparison with the correlation graphs. This approach isolates the impact of the ensemble method itself, allowing us to directly evaluate its effectiveness relative to the simpler correlation-based representation.

Since (1) is the difference of two probabilities, it can be seen from it that the resulting edge weight w_{ij} ranges between -1 and 1 :

- Negative weights ($w_{ij} < 0$) indicated that brain state 1 is more likely.
- Positive weights ($w_{ij} > 0$) indicated that brain state 2 is more likely.
- Larger absolute values ($|w_{ij}|$) signified higher informativeness for classification.

Each edge required training an individual machine learning model to compute the probabilities in (1). In our study, we used the implementation of logistic regression from scikit-learn [28] with default parameters, including a regularization parameter $C = 1.0$, ℓ_2 -regularization penalty, 'lbfgs' optimization solver, and a maximum of 100 iterations. The entire pipeline of using a set of basic models to construct a graph and then using the metamodel for the final classification can be observed in Fig. 1. The metamodels themselves will be discussed in sections II-D and II-E.

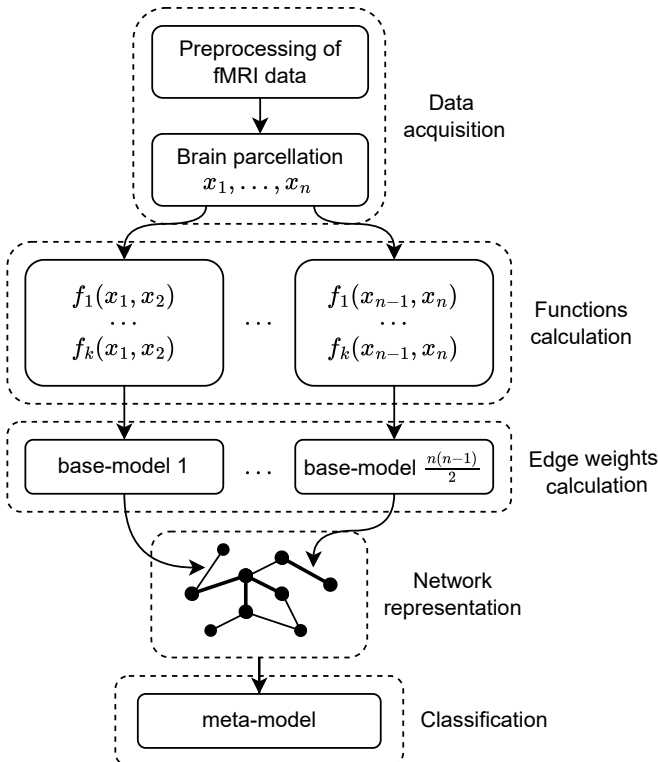


Fig. 1. Pipeline of ensemble graph contraction and classification.

To meet the requirements of graph neural networks, the vertex values h_i were set to a constant $h_i = 1$, as the edge weights encapsulate all information from the brain region time series.

C. Cross-Validation Procedure.

The cross-validation process was designed to account for the two levels of training in our pipeline: the base-models (logistic regressions) used to construct the graphs and the meta-models (logistic regression or a graph neural network) used for classification. Below is a detailed description of the algorithm we devised (Algorithm 1).

Algorithm 1: Cross-Validation Procedure

Input: Dataset D , Number of groups $G = 4$

Output: Performance metrics

Split D into G groups: D_1, D_2, \dots, D_G ;

foreach $i \in \{1, 2, \dots, G\}$ **do**

$D_i \leftarrow$ test set for meta-model;

$D_{\text{meta-train}} \leftarrow \{D_j \mid j \neq i\}$;

foreach $j \in \{1, 2, \dots, G\} \setminus \{i\}$ **do**

$D_j \leftarrow$ set for graph construction;

$D_{\text{base-train}} \leftarrow \{D_k \mid k \neq i, k \neq j\}$;

Train base-models on $D_{\text{base-train}}$;

Compute graphs for D_j using the trained base-models;

end

Retrain base-models on $D_{\text{meta-train}}$;

Compute graphs for D_i using the retrained base-models;

Train meta-model on graphs from $D_{\text{meta-train}}$;

Test meta-model on graphs from D_i ;

end

To begin, the dataset of parceled fMRI was randomly divided into four groups to ensure an even distribution of samples. In the outer loop, each group i was sequentially selected as the test set for the meta-model, while the remaining three groups formed the training set for the meta-model. Within this training set for the meta-model, an inner loop was employed to train the base-models responsible for graph construction and then to construct graphs. For each group j within the three training groups, j was used for graph contraction, while the remaining two groups served as the training set for the base-models. The base-models were trained on the parceled fMRI data from these two groups, and graphs were constructed for the group j . After completing the inner loop, the base-models were retrained on the parceled fMRI data from all three groups designated for training the meta-model (graphs have already been constructed for them). These retrained base-models were then used to construct graphs for the test group i . Subsequently, the meta-model was trained on the graphs from the three training groups and evaluated on the graphs from the test group i .

This cross-validation strategy ensured a clear separation between training and testing data for both levels of models,

effectively preventing data leakage. The structure of this algorithm enabled a robust evaluation of the classification performance.

D. Classification Based on Mean Incident Edge Weights of Ensemble Graphs

To perform the classification using ensemble graphs, we calculated the mean incident edge weight $d_i = \frac{1}{378} \sum_{j,j \neq i} w_{ij}$ for each vertex i . The mean incident edge weight of a vertex is computed by averaging the weights of all edges between that vertex and all other vertices in the graph. This process resulted in 379 values, corresponding to the 379 vertices in the graph, as the brain was parcellated into 379 regions. These average weight values were then fed into a logistic regression classifier, which was trained using the default parameters from its implementation in scikit-learn, as detailed in section II-B.2. For model validation, we performed four-fold cross-validation (see Algorithm 1).

The weight of an edge can be interpreted as the confidence in the brain state derived from the data of the two brain regions. Therefore, the mean incident weight of a vertex is the confidence in the brain state obtained by averaging pairwise integrations of the data of this vertex and all other vertices in the graph. Thus this approach allows us to significantly reduce the dimensionality of the graph by considering the number of edges in the complete graph.

E. Comparison of Ensemble and Correlation Graphs with GNN.

We employ a Graph Neural Network built from repeating units we call GCNBlocks (Fig. 2). Each GCNBlock begins with a graph convolutional layer (GCNConv), which aggregates information from node's neighbors according to the graph adjacency structure [29]. Immediately following convolution, we apply a ReLU activation [30] and Batch Normalization [31] to improve convergence and stabilize training. A Dropout layer then randomly deactivates a fraction of the feature channels, reducing overfitting by preventing the network from relying too heavily on any single neuron [32]. To preserve and fuse information across depths, each GCNBlock incorporates a skip connections [33]. Within each GCNBlock we concatenate the block's new features with the previous block's Dropout output (or, for the first block, with the original node features): specifically, GCNBlock 1 fuses its post-dropout features with the original input node features; GCNBlock 2 fuses its post-dropout features with GCNBlock 1's post-dropout features; and GCNBlock 3 fuse its post-dropout features with GCNBlock 2's post-dropout features.

We stack three GCNBlocks in sequence. After the final block, a global max-pooling operation [34] reduces all node embeddings into a single, fixed-length vector by taking the maximum activation over nodes for each feature channel. This pooled graph representation is then passed through a Batch Normalization layer, ensuring that its distribution remains well-conditioned before entering the classification head. A fully connected layer maps the normalized embedding into the target prediction space, and a sigmoid activation produces a

probability in [0,1] for binary classification. Training is driven by the binary cross-entropy loss.

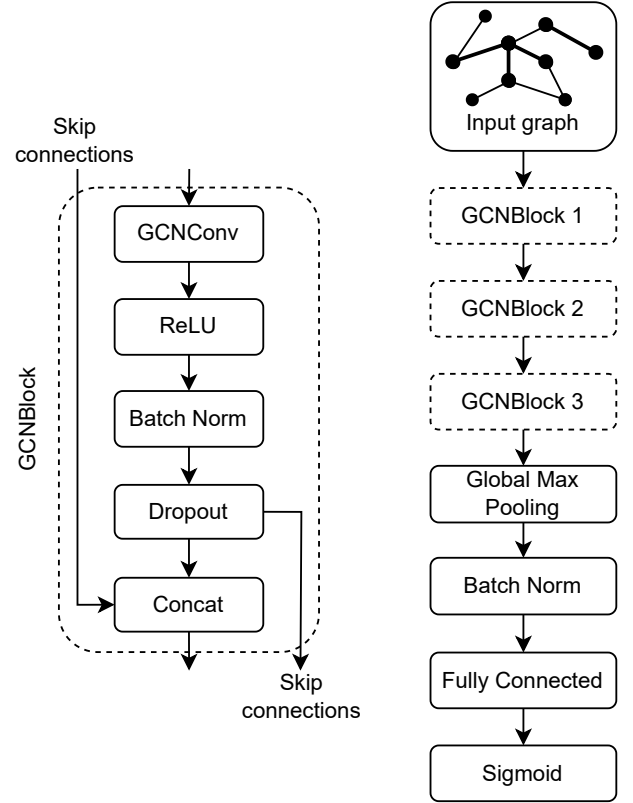


Fig. 2. Architecture of the GNN used to compare the efficiency of ensemble and correlation graphs in a classification task.

To optimize performance without over-smoothing node representations, we found that three convolutional blocks strike the right balance: they extend the receptive field beyond immediate neighbors while avoiding excessive feature homogenization. During training, we used an Adam optimizer [35] with hyperparameters determined on a small hold-out set. To further enhance convergence and combat overfitting, we apply a LinearLR scheduler that linearly decays the learning rate over the total number of iterations. The network was trained for each experiment out of seven possible ones and for each graph type out of two possible ones separately. In training and testing the network, the samples was balanced so that the network simultaneously received data from two classes of the same individuals. That is, if the sample D contains a graph of one state of one experiment of individual j , the sample will also contain a graph of the same individual j of a different state.

For model validation, we performed four-fold cross-validation (see Algorithm 1). In each fold, the network was trained for 100 epochs, and to account for randomness we repeated this process 10 times with different random seeds. From these runs we compute mean values and standard deviations of Accuracy and ROC-AUC. To quantify uncertainty in the difference between our ensemble-based graphs and traditional correlation-based graphs, we build percentile-t confidence intervals by drawing 100 bootstrap samples from

the 40 run-level metric differences [36].

III. RESULTS

For each experiment, 1162 ensemble graphs were constructed, comprising 581 graphs for each brain state (Table I). Additionally, the same number of correlation graphs was constructed for comparison. These graphs were built for two types of parcellation: (1) the time series of each brain region were averaged, (2) the first principal component obtained through PCA was used as the representative time series for each region. Each graph included 379 vertices, corresponding to brain regions obtained through parcellation, and 71631 edges describing relationships between these regions.

A. Classification Based on Mean Incident Edge Weights of Ensemble Graphs.

Using the ensemble graphs with log regression, we achieved an average classification accuracy ranging from 97.07% to 99.74% for mean parcellation method and from 96.73% to 99.40% for pca parcellation method. Classification accuracy for all experiments was higher for mean parcellation method. Table II summarizes classification accuracy and receiver operating characteristic area under the curve metric (ROC AUC) for the seven experiments and two parcellation methods in the format “mean (standard deviation).”

TABLE II

CLASSIFICATION RESULTS BASED ON MEAN INCIDENT WEIGHTS OF VERTICES WITH LOGISTIC REGRESSION FOR SEVEN TASKS AND TWO PARCELLATION METHODS.

		Accuracy, %	ROC AUC, %
Working Memory	mean	98.19 (0.86)	99.88 (0.03)
	pca	97.42 (0.58)	99.78 (0.04)
Gambling	mean	97.07 (0.39)	99.20 (0.32)
	pca	96.73 (0.72)	99.19 (0.46)
Motor Activity	mean	99.57 (0.28)	99.99 (0.01)
	pca	98.54 (0.95)	99.96 (0.04)
Language Processing	mean	99.74 (0.29)	100.00 (0.01)
	pca	99.31 (0.42)	99.99 (0.01)
Social Cognition	mean	99.48 (0.17)	100.00 (0.00)
	pca	99.40 (0.29)	99.99 (0.01)
Relational Processing	mean	98.11 (0.52)	99.89 (0.08)
	pca	97.68 (1.20)	99.81 (0.12)
Emotion Processing	mean	98.45 (1.04)	99.76 (0.23)
	pca	97.42 (0.99)	99.65 (0.25)

B. Comparison of Ensemble and Correlation Graphs with GNN.

Since the average classification accuracy using logistic regression was found to be higher for mean parcellation method, we took only graphs obtained using this method to compare the two types of graphs. Using GNN, we achieved an average classification accuracy ranging from 88.00% to 99.42% for ensemble graphs and from 61.86% to 97.94% for correlation graphs. In all experiments, the best classification accuracy was obtained using ensemble graphs. Table III summarizes classification accuracy and receiver operating characteristic area under the curve metric (ROC AUC) for the seven experiments in the format “mean (standard deviation).”

TABLE III

CLASSIFICATION RESULTS BASED ON GNN FOR CORRELATION AND ENSEMBLE GRAPHS FOR MEAN PARCELLATION METHOD.

		Correlation	Ensemble
Working Memory	Accuracy, %	80.36 (2.06)	97.46 (1.46)
	ROC AUC, %	88.02 (2.16)	99.73 (0.30)
Gambling	Accuracy, %	72.27 (3.90)	93.87 (1.56)
	ROC AUC, %	79.98 (3.51)	98.11 (0.77)
Motor	Accuracy, %	77.96 (3.29)	98.63 (1.11)
	ROC AUC, %	84.97 (2.83)	99.92 (0.12)
Language Processing	Accuracy, %	97.94 (1.23)	99.42 (0.51)
	ROC AUC, %	99.78 (0.26)	99.98 (0.06)
Social Cognition	Accuracy, %	88.40 (2.07)	98.90 (0.63)
	ROC AUC, %	95.07 (1.50)	99.93 (0.11)
Relational Processing	Accuracy, %	83.17 (2.69)	94.90 (2.24)
	ROC AUC, %	91.33 (2.52)	99.25 (0.50)
Emotion Processing	Accuracy, %	61.86 (3.45)	88.00 (2.40)
	ROC AUC, %	65.01 (4.24)	95.12 (1.77)

To quantify uncertainty in the difference between our ensemble-based graphs and traditional correlation-based graphs, we build percentile-t confidence intervals by drawing 100 bootstrap samples from the 40 run-level metric differences. In our comparative plots (Fig. 3), the horizontal axis shows the percentage-point difference (ensemble minus correlation) for each metric with circles, the vertical lines indicate the mean differences, and the horizontal bars denote the percentile-t intervals for mean differences. Intervals entirely above zero are colored green (ensemble graph significantly better), those crossing zero are gray (no significant difference), and those entirely below zero are red (correlation graph significantly better); individual run-level differences are overlaid as circles. In all experiments, ensemble graphs lead to statistically significantly better classification results

C. Visualization.

To represent graphs in a plane, we used two methods to visualize ensemble graphs: (1) heat maps for edge weight matrices and (2) Fruchterman-Reingold force-directed algorithm [37]. Since better classification results were achieved using the parcellation method based on the averaging of time series within brain regions, all visualizations presented in this article correspond exclusively to this method. In addition, the visualizations were generated by averaging the edge weights across all individuals in the meta-level test sets obtained during cross-validation.

Fig. 4 presents the averaged edge weight matrices of ensemble graphs for two brain states in the language processing experiment, specifically “story” and “math” tasks. The edge weights are color-coded: blue represents negative weights, indicating a stronger association with brain state 1, while red represents positive weights, reflecting a stronger association with brain state 2. The horizontal and vertical axes correspond to the indices of brain regions defined by the HCP MMP atlas.

In Fig. 5, we demonstrate the application of the Fruchterman-Reingold force-directed algorithm, implemented with default parameters from the networkx library [38], to the averaged edge weight matrices of ensemble graphs for two brain states in the language processing experiment. To ensure clarity, the edges themselves are not drawn, as the number of

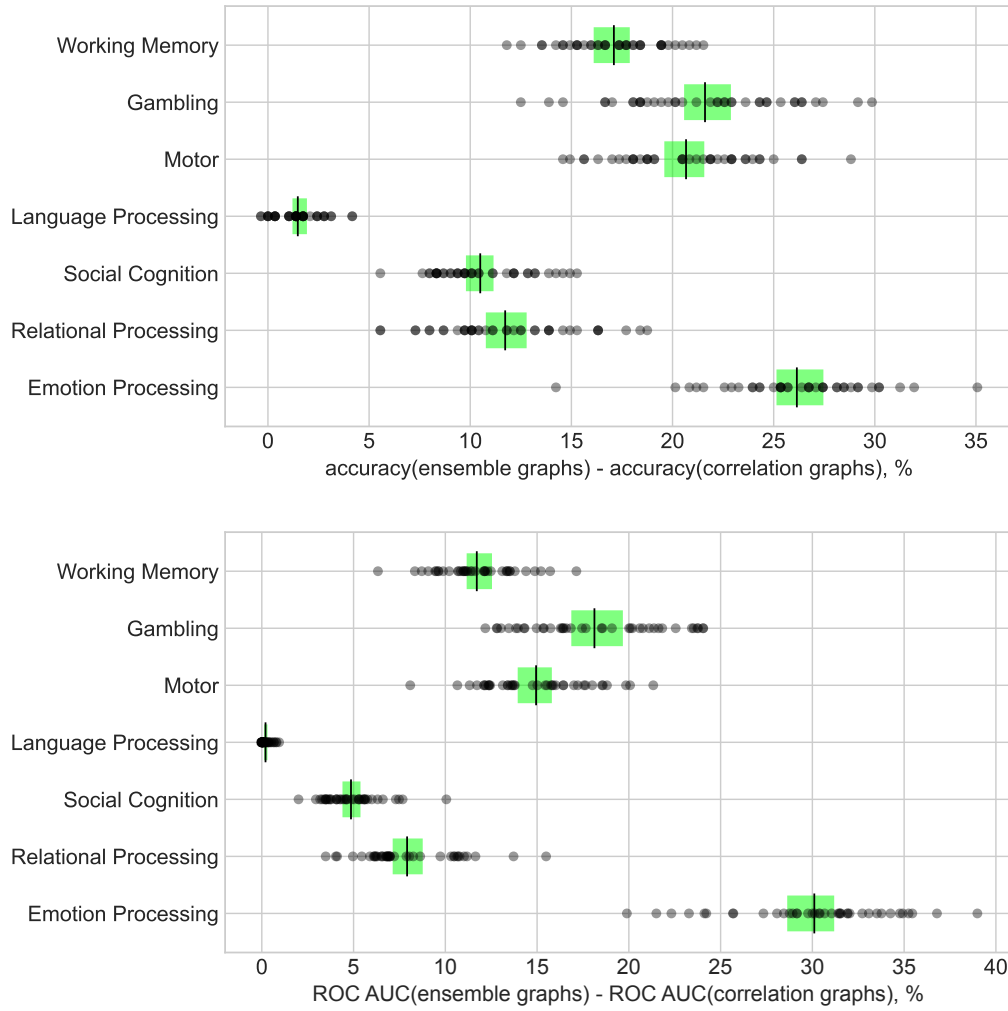


Fig. 3. Bootstrap percentile-t confidence intervals for run-level metric differences between ensemble-based and correlation-based graphs.

edges in the complete graph is too large for the visualization to remain interpretable. However, the edge weights are still accounted for in the positioning of the vertices, meaning that the layout reflects their relative influence. Colors of the vertices correspond to the colors of brain regions as defined by the [27] multi-modal parcellation atlas. The size of each vertex is determined as follows. The difference between the mean incident edge weights of a vertex in the two brain states is first calculated. This difference is then scaled by a multiplier z and raised to an exponential power. The scaling ensures that the largest vertex size matches the maximum value of 200 for the `node_size` parameter in `draw_networkx_nodes` function. The exponential transformation highlights differences more distinctly, making variations between regions visually clearer.

In both cases of visualization it can be seen that some regions stand out as more important for classification. In the case of matrices, such regions give rise to strongly shaded lines. In the case of graphs themselves, the vertices representing such regions are large and close to the center in one of the states (when edge weights tend to be positive).

IV. DISCUSSION

In this work, we proposed a method for representing fMRI data in network form with ensemble learning approach. We tested the method using a simple logistic-regression classifier on the mean incident edge weights. The results demonstrate the outstanding effectiveness of the method: in binary brain-state classification across seven experiments, accuracy ranged from 97.07 % to 99.74 %. Even a simple model based on the mean incident edge weights exhibits high discriminative power (up to 99.74 % accuracy), indicating that key information on brain state is already encoded in the global graph topology. For comparison, traditional correlation graphs processed with GNN yielded only 61.86 %–97.94 % accuracy, whereas the ensemble graphs achieved 88.00 %–99.42 % with the same GNN architecture. So ensemble graphs outperform their correlation-only counterparts by an average of 15.60 % in accuracy, highlighting their potential.

We hypothesize that GNN achieved a worse result than logistic regression for ensemble graphs due to (1) the insufficient number of graphs to train it, since we did not perform data augmentation to increase the sample size, and (2) we did not conduct an extensive study to determine the optimal

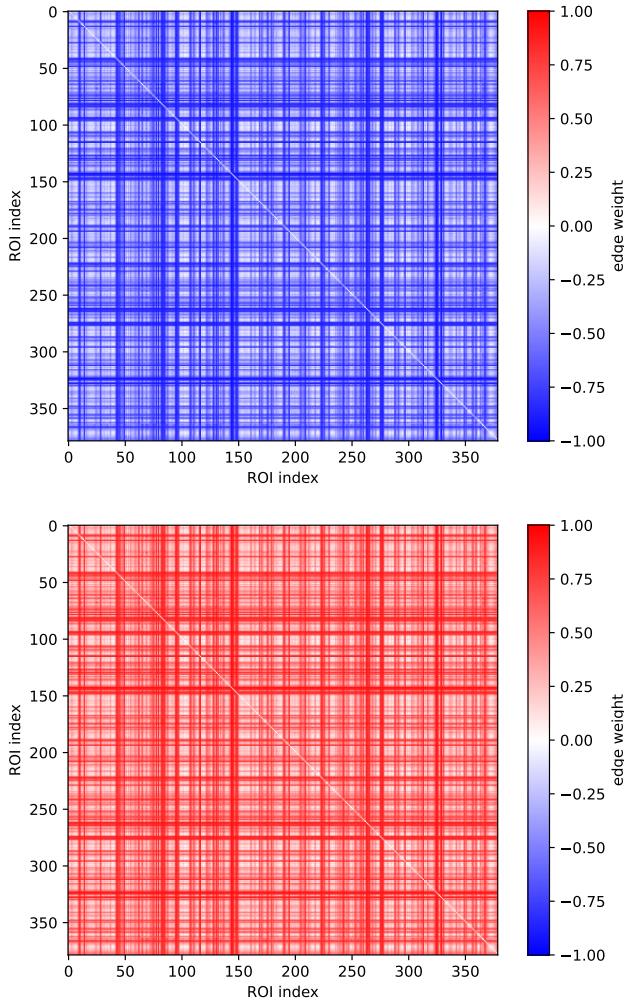


Fig. 4. Averaged edge weight matrices of ensemble graphs for “story” (top) and “math” (bottom) brain states in the language processing experiment.

architecture for the GNN. We did not do this because the main goal of this study was to propose a new method of graph-based fMRI representation using machine learning. And selection of an optimal metamodel and integration of it with our method is a separate and complex task.

A. Interpretability.

First of all, ensemble graph is a method of generating features in the network structure for further classification. It is possible to apply the interpretation about brain state confidence at the level of graph edges, which was described in subsection II-D. Then it is possible to search for connections, brain regions and communities of regions important for classification when examining the graph structure in detail. In this way, the huge potential of applying of various network analysis methods to this type of graphs is revealed.

B. Relation of Our HCP Data Classification Task to the Existing Literature.

Network-based methods have previously been applied to HCP fMRI data for classification tasks. In this section, we

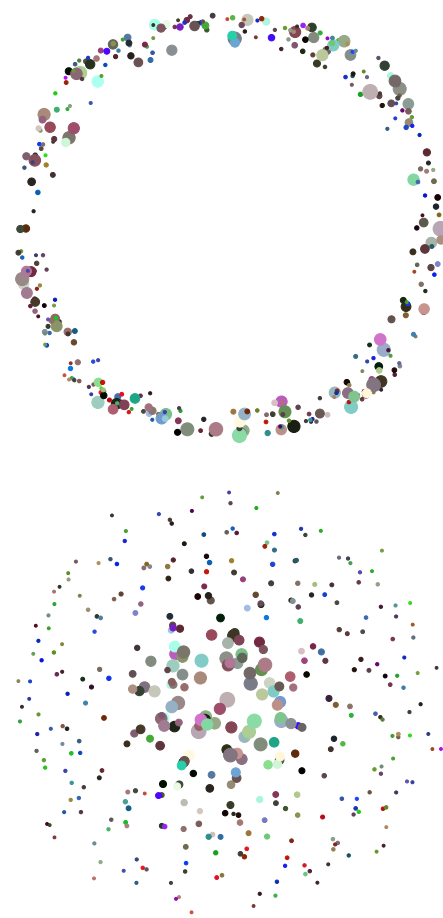


Fig. 5. Application of the Fruchterman-Reingold force-directed algorithm to the averaged edge weight matrices of ensemble graphs for “story” (top) and “math” (bottom) brain states in the language processing experiment.

outline how the classification problem addressed in the present work differs from those tackled earlier in the literature.

In [12], the authors developed an interpretable BrainGNN model with a mechanism for selecting significant regions. They used correlation-based graphs to represent the data. Their model performed well in distinguishing among seven HCP fMRI experiments, achieving an average classification accuracy of 94.4%.

A similar classification task on HCP fMRI data using correlation-based representations was tackled by [10]. The authors proposed a GNN model with three convolutional layers that employed various node embedding techniques (NetMF, Node2Vec, etc.) to capture the network topology; this model reached an accuracy of 97.7% with optimal hyperparameters.

In [39], the authors demonstrated multi-state classification across 21 states from six HCP cognitive experiments using a GNN. In their approach, they first constructed a brain network from resting-state fMRI and then superimposed task-fMRI dynamics on that network. They achieved a mean accuracy of 89.8%.

In contrast, our work uses only task-fMRI and focuses on binary classification for each of the seven HCP experiments. We

did not aim to maximize accuracy for a different classification formulation. Rather, our primary goal was to propose a novel method and demonstrate its effectiveness with minimal effort and complexity, relying, for example, on a logistic regression baseline rather than deep neural networks.

C. Future directions.

1) Methodological Perspectives: In this study, we employed logistic regression as our base model. However, generally any probabilistic classification method can be used: from support vector machine [40] to perceptron [41]. The key requirement is that the models remain sufficiently simple to train on small samples, given the size of typical neuroscience datasets.

While this work focuses on a binary classification task, our approach can be readily adapted for multiclass classification by replacing the base models accordingly. For example, using multiple logistic regression would assign each edge a weight vector reflecting confidence in each possible brain state. It is also possible to reformulate the problem as a regression task by employing regression models (e.g., a linear regression model) rather than classifiers.

Moreover, as noted above, we propose representing generated features in a graph format, opening substantial potential for applying and adapting existing network-analysis techniques to these kinds of graphs within cognitive neuroscience.

Selecting an appropriate meta-model remains a challenging but critical task. We see great promise in graph-based machine learning methods, naturally aligned with the network representation of the data, as well as in explainable AI techniques [42]–[44] for automated selection of the most informative connections, regions, and communities.

2) Perspectives for Other Neuroimaging Modalities: Although this work concentrates on fMRI data, the proposed approach can be extended to other neuroimaging modalities. For high-frequency EEG/MEG data, one could leverage frequency-domain characteristics of regions (e.g. band-power [45]) and more sophisticated connectivity metrics (e.g. Coherency [46], Phase Locking Value [47]), when computing edge weights. Furthermore, multimodal integration, such as simultaneous EEG and fMRI recordings, becomes feasible by solving the EEG inverse problem [48] to map sensor data into source space, then applying a consistent brain parcellation across both modalities. This strategy would combine the temporal resolution advantage of EEG with the spatial resolution advantage of fMRI within a single network representation.

3) Applications to Pathological Brain States: Although our study focused on classifying cognitive states, the same methodology can be applied to the classification of pathological brain conditions. Future work may explore its utility in distinguishing between healthy and disease-related network alterations, potentially aiding in the diagnosis and monitoring of neurological disorders.

D. Code availability

The code that constructs ensemble graphs, implements cross validation and performs training and testing of meta-models, including logistic regression and graph

neural network, is available at <https://github.com/Daniil-Vlasenko/EnsGraph2025.git>.

REFERENCES

- [1] P. S. Kostenetskiy, R. A. Chulkevich, and V. I. Kozyrev, "HPC Resources of the Higher School of Economics," *Journal of Physics: Conference Series*, vol. 1740, no. 1, p. 012050, Jan. 2021. DOI: 10.1088/1742-6596/1740/1/012050.
- [2] A. Craik, Y. He, and J. L. Contreras-Vidal, "Deep learning for electroencephalogram (EEG) classification tasks: A review," *Journal of Neural Engineering*, vol. 16, no. 3, p. 031001, Jun. 2019. DOI: 10.1088/1741-2552/ab0ab5.
- [3] I. Saranskaia, B. Gutkin, and D. Zakharov, "Aim-based choice of strategy for MEG-based brain state classification," *The European Physical Journal Special Topics*, Mar. 22, 2025. DOI: 10.1140/epjs/s11734-025-01587-y.
- [4] D. Vaghari, E. Kabir, and R. N. Henson, "Late combination shows that MEG adds to MRI in classifying MCI versus controls," *NeuroImage*, vol. 252, p. 119054, May 15, 2022. DOI: 10.1016/j.neuroimage.2022.119054.
- [5] D. J. Heeger and D. Ress, "What does fMRI tell us about neuronal activity?" *Nature Reviews Neuroscience*, vol. 3, no. 2, pp. 142–151, Feb. 2002. DOI: 10.1038/nrn730.
- [6] N. K. Logothetis, "What we can do and what we cannot do with fMRI," *Nature*, vol. 453, no. 7197, pp. 869–878, Jun. 2008. DOI: 10.1038/nature06976.
- [7] J. Wang, X. Zuo, and Y. He, "Graph-based network analysis of resting-state functional MRI," *Frontiers in Systems Neuroscience*, vol. 4, Jun. 7, 2010. DOI: 10.3389/fnsys.2010.00016.
- [8] J. Richiardi, H. Eryilmaz, S. Schwartz, P. Vuilleumier, and D. Van De Ville, "Decoding brain states from fMRI connectivity graphs," *NeuroImage*, Multivariate Decoding and Brain Reading, vol. 56, no. 2, pp. 616–626, May 15, 2011. DOI: 10.1016/j.neuroimage.2010.05.081.
- [9] S. Takerkart, G. Auzias, B. Thirion, and L. Ralaivola, "Graph-Based Inter-Subject Pattern Analysis of fMRI Data," *PLOS ONE*, vol. 9, no. 8, e104586, Aug. 15, 2014. DOI: 10.1371/journal.pone.0104586.
- [10] M. Saeidi, W. Karwowski, F. V. Farahani, et al., "Decoding Task-Based fMRI Data with Graph Neural Networks, Considering Individual Differences," *Brain Sciences*, vol. 12, no. 8, p. 1094, Aug. 17, 2022. DOI: 10.3390/brainsci12081094.
- [11] X. Li, N. C. Dvornek, Y. Zhou, J. Zhuang, P. Ventola, and J. S. Duncan, "Graph Neural Network for Interpreting Task-fMRI Biomarkers," *Medical image computing and computer-assisted intervention : MICCAI ... International Conference on Medical Image Computing and Computer-Assisted Intervention*, vol. 11768, pp. 485–493, Oct. 2019. DOI: 10.1007/978-3-030-32254-0_54.
- [12] X. Li, Y. Zhou, N. Dvornek, et al., "BrainGNN: Interpretable Brain Graph Neural Network for fMRI Analysis," *Medical Image Analysis*, vol. 74, p. 102233, Dec. 1, 2021. DOI: 10.1016/j.media.2021.102233.
- [13] A. Bessadok, M. A. Mahjoub, and I. Rekik, "Graph Neural Networks in Network Neuroscience," *IEEE Transactions on Pattern Analysis and Machine Intelligence*, vol. 45, no. 5, pp. 5833–5848, May 1, 2023. DOI: 10.1109/TPAMI.2022.3209686.
- [14] A. N. Gorban, T. A. Tyukina, L. I. Pokidysheva, and E. V. Smirnova, "Dynamic and thermodynamic models of adaptation," *Physics of Life Reviews*, vol. 37, pp. 17–64, Jul. 1, 2021. DOI: 10.1016/j.plrev.2021.03.001.
- [15] M. Ursino, G. Ricci, and E. Magosso, "Transfer Entropy as a Measure of Brain Connectivity: A Critical Analysis With the Help of Neural Mass Models," *Frontiers in Computational Neuroscience*, vol. 14, Jun. 5, 2020. DOI: 10.3389/fncom.2020.00045.
- [16] J. Hlinka, M. Paluš, M. Vejmelka, D. Mantini, and M. Corbetta, "Functional connectivity in resting-state fMRI: Is linear correlation sufficient?" *NeuroImage*, vol. 54, no. 3, pp. 2218–2225, Feb. 1, 2011. DOI: 10.1016/j.neuroimage.2010.08.042.
- [17] A. Roebroeck, E. Formisano, and R. Goebel, "Mapping directed influence over the brain using Granger causality and fMRI," *NeuroImage*, vol. 25, no. 1, pp. 230–242, Mar. 1, 2005. DOI: 10.1016/j.neuroimage.2004.11.017.

- [18] D. Vlasenko, A. Zaikin, and D. Zakharov, "Ensemble methods for representation of fMRI, EEG/MEG data in graph form for classification of brain states," in *2024 8th Scientific School Dynamics of Complex Networks and Their Applications (DCNA)*, Kaliningrad, Russian Federation: IEEE, Sep. 19, 2024, pp. 258–261. DOI: 10.1109/DCNA63495.2024.10718443.
- [19] M. A. Ganaie, M. Hu, A. K. Malik, M. Tanveer, and P. N. Suganthan, "Ensemble deep learning: A review," *Engineering Applications of Artificial Intelligence*, vol. 115, p. 105151, Oct. 1, 2022. DOI: 10.1016/j.engappai.2022.105151.
- [20] A. Mohammed and R. Kora, "A comprehensive review on ensemble deep learning: Opportunities and challenges," *Journal of King Saud University - Computer and Information Sciences*, vol. 35, no. 2, pp. 757–774, Feb. 1, 2023. DOI: 10.1016/j.jksuci.2023.01.014.
- [21] M. Galar, A. Fernandez, E. Barrenechea, H. Bustince, and F. Herrera, "A Review on Ensembles for the Class Imbalance Problem: Bagging-, Boosting-, and Hybrid-Based Approaches," *IEEE Transactions on Systems, Man, and Cybernetics, Part C (Applications and Reviews)*, vol. 42, no. 4, pp. 463–484, Jul. 2012. DOI: 10.1109/TSMCC.2011.2161285.
- [22] T. Nazarenko, H. J. Whitwell, O. Blyuss, and A. Zaikin, "Parenclitic and Synolytic Networks Revisited," *Frontiers in Genetics*, vol. 12, p. 733783, Oct. 20, 2021. DOI: 10.3389/fgene.2021.733783.
- [23] J. S. Elam, M. F. Glasser, M. P. Harms, *et al.*, "The Human Connectome Project: A retrospective," *NeuroImage*, vol. 244, p. 118543, Dec. 2021. DOI: 10.1016/j.neuroimage.2021.118543.
- [24] D. C. V. Essen, S. M. Smith, D. M. Barch, *et al.*, "The WU-Minn Human Connectome Project: An Overview," *NeuroImage*, vol. 80, p. 62, Oct. 10, 2013. DOI: 10.1016/j.neuroimage.2013.05.041.
- [25] D. M. Barch, G. C. Burgess, M. P. Harms, *et al.*, "Function in the human connectome: Task-fMRI and individual differences in behavior," *NeuroImage*, Mapping the Connectome, vol. 80, pp. 169–189, Oct. 15, 2013. DOI: 10.1016/j.neuroimage.2013.05.033.
- [26] M. F. Glasser, S. N. Sotiropoulos, J. A. Wilson, *et al.*, "The minimal preprocessing pipelines for the Human Connectome Project," *NeuroImage*, Mapping the Connectome, vol. 80, pp. 105–124, Oct. 15, 2013. DOI: 10.1016/j.neuroimage.2013.04.127.
- [27] M. F. Glasser, T. S. Coalson, E. C. Robinson, *et al.*, "A multi-modal parcellation of human cerebral cortex," *Nature*, vol. 536, no. 7615, pp. 171–178, Aug. 2016. DOI: 10.1038/nature18933.
- [28] F. Pedregosa, G. Varoquaux, A. Gramfort, *et al.*, "Scikit-learn: Machine Learning in Python," *Journal of Machine Learning Research*, vol. 12, no. 85, pp. 2825–2830, 2011.
- [29] T. N. Kipf and M. Welling, "Semi-Supervised Classification with Graph Convolutional Networks," (Feb. 22, 2017), pre-published.
- [30] V. Nair and G. E. Hinton, "Rectified linear units improve restricted boltzmann machines," in *Proceedings of the 27th International Conference on International Conference on Machine Learning*, ser. ICML'10, Madison, WI, USA: Omnipress, Jun. 21, 2010, pp. 807–814.
- [31] S. Ioffe and C. Szegedy, "Batch Normalization: Accelerating Deep Network Training by Reducing Internal Covariate Shift," (Mar. 2, 2015), pre-published.
- [32] N. Srivastava, G. Hinton, A. Krizhevsky, I. Sutskever, and R. Salakhutdinov, "Dropout: A Simple Way to Prevent Neural Networks from Overfitting," *Journal of Machine Learning Research*, vol. 15, no. 56, pp. 1929–1958, 2014.
- [33] K. He, X. Zhang, S. Ren, and J. Sun, "Deep Residual Learning for Image Recognition," (Dec. 10, 2015), pre-published.
- [34] K. Xu, W. Hu, J. Leskovec, and S. Jegelka, "How Powerful are Graph Neural Networks?" (Feb. 22, 2019), pre-published.
- [35] D. P. Kingma and J. Ba, "Adam: A Method for Stochastic Optimization," (Jan. 30, 2017), pre-published.
- [36] B. Efron and R. J. Tibshirani, *An Introduction to the Bootstrap*. New York: Chapman and Hall/CRC, May 15, 1994, 456 pp. DOI: 10.1201/9780429246593.
- [37] T. M. J. Fruchterman and E. M. Reingold, "Graph drawing by force-directed placement," *Software: Practice and Experience*, vol. 21, no. 11, pp. 1129–1164, 1991. DOI: 10.1002/spe.4380211102.
- [38] A. A. Hagberg, D. A. Schult, and P. J. Swart, "Exploring Network Structure, Dynamics, and Function using NetworkX," *scipy*, May 6, 2008. DOI: 10.25080/TCWV9851.
- [39] Y. Zhang, N. Farrugia, and P. Bellec, "Deep learning models of cognitive processes constrained by human brain connectomes," *Medical Image Analysis*, vol. 80, p. 102507, Aug. 1, 2022. DOI: 10.1016/j.media.2022.102507.
- [40] C. Cortes and V. Vapnik, "Support-vector networks," *Machine Learning*, vol. 20, no. 3, pp. 273–297, Sep. 1, 1995. DOI: 10.1007/BF00994018.
- [41] F. Rosenblatt, "The perceptron: A probabilistic model for information storage and organization in the brain," *Psychological Review*, vol. 65, no. 6, pp. 386–408, 1958. DOI: 10.1037/h0042519.
- [42] Z. Ying, D. Bourgeois, J. You, M. Zitnik, and J. Leskovec, "GN-Explainer: Generating Explanations for Graph Neural Networks," in *Advances in Neural Information Processing Systems*, vol. 32, Curran Associates, Inc., 2019.
- [43] D. Luo, W. Cheng, D. Xu, *et al.*, "Parameterized Explainer for Graph Neural Network," *Advances in Neural Information Processing Systems*, vol. 33, pp. 19620–19631, 2020.
- [44] H. Yuan, J. Tang, X. Hu, and S. Ji, "XGNN: Towards Model-Level Explanations of Graph Neural Networks," in *Proceedings of the 26th ACM SIGKDD International Conference on Knowledge Discovery & Data Mining*, ser. KDD '20, New York, NY, USA: Association for Computing Machinery, Aug. 20, 2020, pp. 430–438. DOI: 10.1145/3394486.3403085.
- [45] P. Welch, "The use of fast Fourier transform for the estimation of power spectra: A method based on time averaging over short, modified periodograms," *IEEE Transactions on Audio and Electroacoustics*, vol. 15, no. 2, pp. 70–73, Jun. 1967. DOI: 10.1109/TAU.1967.1161901.
- [46] G. Nolte, O. Bai, L. Wheaton, Z. Mari, S. Vorbach, and M. Hallett, "Identifying true brain interaction from EEG data using the imaginary part of coherency," *Clinical Neurophysiology: Official Journal of the International Federation of Clinical Neurophysiology*, vol. 115, no. 10, pp. 2292–2307, Oct. 2004. DOI: 10.1016/j.clinph.2004.04.029.
- [47] J. P. Lachaux, E. Rodriguez, J. Martinerie, and F. J. Varela, "Measuring phase synchrony in brain signals," *Human Brain Mapping*, vol. 8, no. 4, pp. 194–208, 1999. DOI: 10.1002/(sici)1097-0193(1999)8:4<194::aid-hbm4>3.0.co;2-c.
- [48] M. S. Hämmäläinen and R. J. Ilmoniemi, "Interpreting magnetic fields of the brain: Minimum norm estimates," *Medical & Biological Engineering & Computing*, vol. 32, no. 1, pp. 35–42, Jan. 1994. DOI: 10.1007/BF02512476.